RSC Advances

PAPER

View Article Online
View Journal | View Issue

Cite this: *RSC Adv.*, 2021, **11**, 30148

Synthesis and characterization of a mononuclear zinc(II) Schiff base complex: on the importance of C–H···π interactions†

Tanmoy Basak,[a] Antonio Frontera [b] and Shouvik Chattopadhyay *[a]

Received 20th May 2021
Accepted 24th August 2021

DOI: 10.1039/d1ra03943a

rsc.li/rsc-advances

A zinc(II) complex, $[ZnL(H_2O)]\cdot H_2O$ {H_2L = 2,2′-[(2,2-dimethyl-1,3-propanediyl)bis(nitrilomethylidyne)]bis[6-ethoxyphenol]} has been synthesized and characterized by UV-vis and IR spectroscopy. The structure of the complex has been confirmed by X-ray crystallography and the noncovalent interactions characterized using Hirshfeld surface analysis. In addition to the conventional H-bonds involving the Zn-coordinated and non-coordinated water molecules, interesting C–H···π interactions between the H-atoms belonging to aliphatic part of the ligand (2,2-dimethyl-1,3-propanediyl) and the Zn-coordinated aromatic rings are established. These interactions have been studied using DFT calculations (PBE0-D3/def2-TZVP) and characterized using molecular electrostatic potential (MEP) surfaces and the noncovalent interaction (NCI) plot index analyses.

Introduction

Zinc(II) complexes have lots of important applications as useful electronic and opto-electronic materials.[1–5] Many zinc(II) complexes have also been prepared recently to explore their potential use in photonic devices.[6] The importance of zinc(II) in biology is well known. Several zinc(II) complexes have been shown to have the ability to mimic the active sites of many zinc metalloenzymes.[7–10] Many zinc(II) complexes are shown to have the ability to degrade organic dyes in aqueous solution.[11–13] To show strong fluorescence is a typical behaviour of any zinc(II) complex, and the fluorescence intensity usually decreases in presence of different nitroaromatic compounds.[14–17] So, many zinc(II) complexes have been used for the detection of nitro-aromatic explosives by turn off fluorescence response.[18–20] The d^{10} electronic configuration of zinc(II) also favours a variety of coordination geometries, *e.g.* tetrahedral,[21] square pyramidal,[22] octahedral,[23] trigonal prism,[24] trigonal dodecahedral[25] *etc.* Obviously, tetrahedral is by far the most common geometry of zinc(II). These complexes show varieties of molecular and supramolecular architectures.[26–30]

A variety of supramolecular interactions are responsible for the crystal packing of coordination compounds, leading to a broad range of dimensional frameworks (0D to 3D) through a variety of forces.[31,32] Apart from coordination and hydrogen bonds,[33] forces associated with aromatic π-systems like π-stacking, lone pair···π, ion···π and C–H···π are important guiding the formation of supramolecular polymeric architectures in solid state.[34] In particular, the C–H···π interaction is a weak attraction between a C–H bond and a π-system (aromatic, double or triple bond), and its roles and significance in chemistry and biochemistry have been widely discussed.[35,36]

Salen type N_2O_2 donor Schiff bases have been widely used to synthesize many zinc(II) complexes.[37–40] This manuscript reports the synthesis and X-ray characterization and Hirshfeld surface analysis of a new Zn(II) complex, $[ZnL(H_2O)]\cdot H_2O$ with a salen type Schiff base (H_2L). The structure directing role of C–H···π interactions between the H-atoms belonging to aliphatic part of the ligand (2,2-dimethyl-1,3-propanediyl) and the Zn-coordinated aromatic rings has been studied energetically using DFT calculations at the PBE0-D3/def2-TZVP level of theory. These interactions have been further rationalized using molecular electrostatic potential (MEP) surfaces and characterized using the non-covalent interaction (NCI) plot index analysis.

Experimental section

3-Ethoxysalicylaldehyde, 2,2-dimethylpropane-1,3-diamine, methanol, zinc(II) acetate dihydrate and DMF were commercially available, reagent grade, and used as purchased from Sigma-Aldrich without further purification.

Preparation of ligand

Preparation of H_2L, {2,2′-[(2,2-dimethyl-1,3-propanediyl) bis(nitrilomethylidyne)]bis[6-ethoxyphenol]}. The N_2O_2 donor Schiff base ligand, H_2L, was prepared by refluxing 2,2-

[a]*Department of Chemistry, Inorganic Section, Jadavpur University, Kolkata-700032, India. E-mail: shouvik.chem@gmail.com*

[b]*Departamento de Química, Universitat de les Illes Balears, Crta. de Valldemossa km 7.5, 07122 Palma, Baleares, Spain*

† CCDC 2082611. For crystallographic data in CIF or other electronic format see DOI: 10.1039/d1ra03943a

dimethylpropane-1,3-diamine (0.10 mL, 1 mmol) with 3-ethoxysalicylaldehyde (0.340 g, ~2 mmol) in methanol solution (10 mL) for *ca.* 1 h. It was not isolated, but was used directly for the preparation of the complex.

Preparation of complex

[ZnL(H$_2$O)]·H$_2$O. A methanol solution (10 mL) of zinc(II) acetate dihydrate (0.220 g, ~1 mmol) was added to the methanol solution of the ligand, H_2L and the resulting solution was refluxed for *ca.* 30 min. The resulting solution was kept in open atmosphere for crystallization. Single crystals, suitable for X-ray diffraction, were obtained after few days on slow evaporation of the solution.

Yield: 0.347 g (~70%) based on zinc(II). Colour: yellow; anal. calc. for $C_{23}H_{32}N_2O_6Zn$ (FW 497.88): C, 55.48; H, 6.48; N, 5.63; found: C, 55.44; H, 6.34; N, 5.73%. IR (KBr, cm^{-1}): 1625 ($\nu_{C=N}$), 2840–2960 (ν_{C-H}), 3351 (ν_{O-H}). UV-vis, λ_{max} (nm), [ε_{max} (L mol^{-1} cm^{-1})] (DMF): 232 (6.06×10^3), 272 (2.4×10^3), 356 (7.8×10^2); ^{1}H NMR (DMSO-d_6) δ ppm: 8.12 (s, 2H, –C**H**=N), 6.73 (d, 4H, J = 7.8 Hz, Ar-**H**); 6.26 (t, 2H, J = 7.7 Hz, Ar-**H**); 3.98 (q, 4H, J = 7.0 Hz, –CH$_2$); 3.44 (s, 2H, –CH$_2$); 1.23 (t, 6H, J = 7.0, –CH$_3$); 0.87 (s, 6H, –CH$_3$).

Physical measurement

Elemental analyses (carbon, hydrogen and nitrogen) were performed using a PerkinElmer 240C elemental analyzer. IR spectra in KBr (4500 to 500 cm^{-1}) were recorded with a PerkinElmer Spectrum Two spectrophotometer. Electronic spectra in DMF were recorded on a Shimadzu UV-1700 UV-vis spectrophotometer. The ^{1}H NMR spectra at 400 MHz were recorded in DMSO-d_6 on a JEOL-JNM-ECZ400 S/L1.

X-ray crystallography

Suitable crystals of the complex was used for data collection using a 'Bruker D8 QUEST area detector' diffractometer equipped with graphite-monochromated Mo K$_\alpha$ radiation (λ = 0.71073 Å). The molecular structures were solved by direct method and refined by full-matrix least squares on F^2 using the SHELX-18 package.[41] Non-hydrogen atoms were refined with anisotropic thermal parameters. The hydrogen atoms attached to oxygen atoms of coordinated water molecules were located by difference Fourier maps and were kept at fixed positions. All other hydrogen atoms were placed in their geometrically idealized positions and constrained to ride on their parent atoms. Multi-scan empirical absorption corrections were applied to the data using the program SADABS.[42] The hydrogen atoms attached with the oxygen atoms of lattice water molecules could not be fixed. Crystallographic data and refinement details of the complex are given in Table 1.

Hirshfeld surface analysis

Hirshfeld surfaces[43–45] and the associated two-dimensional (2D) fingerprint[46–48] plots were calculated using Crystal Explorer,[49] with bond lengths to hydrogen atoms set to standard values.[50] Two distances, d_e (the distance from the point to the nearest nucleus external to the surface) and d_i (the distance to the nearest nucleus internal to the surface), are defined for each point on the Hirshfeld surface. The normalized contact distance (d_{norm}) based on d_e and d_i is defined as:

$$d_{norm} = \frac{(d_i - r_i^{vdw})}{r_i^{vdw}} + \frac{(d_e - r_e^{vdw})}{r_e^{vdw}}$$

where r_i^{vdw} and r_e^{vdw} are the van der Waals radii of the atoms. The d_{norm} value is negative or positive depending on intermolecular contacts being shorter or longer than the van der Waals separations. The parameter d_{norm} displays a surface with a red-white-blue colour design, where bright red spots highlight shorter contacts, white areas in the same surface represent contacts around the van der Waals separation and blue regions are devoid of close contacts. For a given CIF, the Hirshfeld surface is said to be unique.[51]

Table 1 Crystal data and refinement details of the complex

Formula	$C_{23}H_{30}N_2O_6Zn$
Formula weight	495.88
Temperature (K)	273
Crystal system	Orthorhombic
Space group	*Aba*2
a (Å)	26.205(11)
b (Å)	25.903(11)
c (Å)	14.652(6)
Z	16
d_{cal} (g cm^{-3})	1.325
μ (mm^{-1})	1.026
F(000)	4160
Total reflection	166 664
Unique reflections	10 962
Observe data [$I > 2\sigma(I)$]	9714
R(int)	0.091
R_1, wR_2 (all data)	0.0564, 0.1327
R_1, wR_2 [$I > 2\sigma(I)$]	0.0450, 0.1204

Theoretical methods

The energies of the assemblies studied herein were computed at the PBE0 (ref. 52)-D3 (ref. 53)/def2-TZVP[54] level of theory using the crystallographic coordinates and the Gaussian-16 program.[55] Grimme's D3 dispersion[53] correction has been used since it is convenient for the correct evaluation of non-covalent interactions where dispersion effects are important like C–H···π interactions. The basis set superposition error for the calculation of interaction energies has been corrected using the counterpoise method.[56] The MEP surfaces have been computed using the same level of theory and plotted using the 0.001 a.u. isosurface. The NCI plot[57] isosurfaces have been used to characterize non-covalent interactions. They correspond to both favorable and unfavorable interactions, as differentiated by the sign of the second density Hessian eigenvalue and defined by the isosurface color. The color scheme is a red-yellow-green-blue scale with red for ρ_{cut}^{+} (repulsive) and blue for ρ_{cut}^{-} (attractive).

Results and discussion

Synthesis

In the present work, a Schiff base ligand, H_2L, was synthesized by the condensation of 2,2-dimethyl-1,3-diaminopropane with

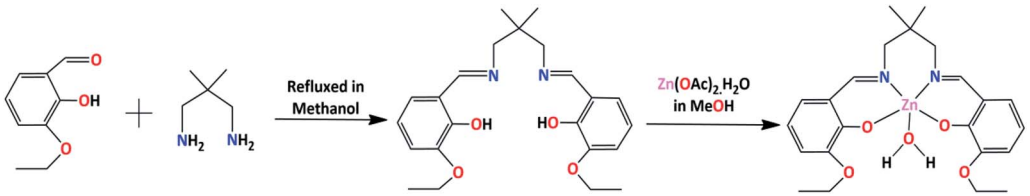

Scheme 1 Synthetic route to the complex. Solvent water molecule has not been shown.

3-ethoxysalicylaldehyde.[58] The ligand was not purified and used directly for preparation of the zinc(II) complex. The reaction of the ligand, H_2L, with zinc(II) acetate in 1 : 1 ratio results the complex. The formation of the complex is shown in Scheme 1.

Description of structures

$[ZnL(H_2O)]\cdot H_2O$. Single crystal X-ray diffraction analysis reveals that the complex crystallizes in orthorhombic space groups, *Aba*2. The asymmetric unit of the complex contains two subunits (A and B) and two non-coordinated water molecules as lattice solvent molecules. Perspective views of both subunits of the complex are shown in Fig. 1. The trigonality indices (τ)[59] of the penta-coordinated zinc(II) centers, Zn(1) and Zn(2), of the complex are 0.411 and 0.375 respectively, which supports the distorted square pyramidal geometries of both zinc(II) centers. The trigonality index (or Addison parameter) of a penta coordinated metal center may be defined as $(a - b)/60$, where a and b are the two largest ligand–metal–ligand angles in the coordination sphere.

In subunit A, the square pyramidal zinc(II) center, Zn(1), resides in the inner N_2O_2 compartment of the di-anion of the compartmental Schiff base ligand, L^{2-}. Two imine nitrogen atoms, N(1) and N(2), and two phenoxo oxygen atoms, O(1) and O(2), of the deprotonated di-Schiff base constitute the equatorial plane. An oxygen atom, O(3), from a water molecule is coordinated in the apical position. Deviations of the coordinating atoms O(1), O(2), N(1), N(2) from the least-square mean planes through them are 0.219(4), −0.219(4), 0.211(4), 0.211(5) Å, respectively. As is usual for square pyramid structures, the zinc(II) is displaced 0.464 Å from the plane towards the apically coordinated oxygen (O3) of the water molecule.

In case of subunit **B**, the zinc(II) center, Zn(2), shows similar coordination mode, in which two imine nitrogen atoms, N(3) and N(4), and two phenoxo oxygen atoms, O(6) and O(7), of the deprotonated di-Schiff base constitute the equatorial plane and an oxygen atom, O(8), from a water molecule is coordinated in the apical position. Deviations of the coordinating atoms O(6), O(7), N(3) and N(4) from the least-square mean planes through them are 0.201, −0.200, −0.194, 0.193 Å, respectively. Here also the zinc(II) is displaced 0.462 Å from the plane towards the apically coordinated oxygen (O8) of the water molecule.

The selected bond lengths and bond angles of the complex are given in Tables 2 and 3 respectively. It is found that Zn(II)–O and Zn(II)–N distances vary from 1.998(4) to 2.037(4) Å and 2.105(5) to 2.121(4) Å, respectively. The bond lengths and angles are comparable with those for the related zinc(II) complexes of the salen type di-Schiff base ligands and are close to the expected values.[7–9,15,16,37–39,58,60] The saturated six membered chelate rings, Zn(1)–N(1)–C(12)–C(11)–C(10)–N(2) {for subunit A} and Zn(1)–N(3)–C(33)–C(35)–C(38)–N(4) {for subunit B},

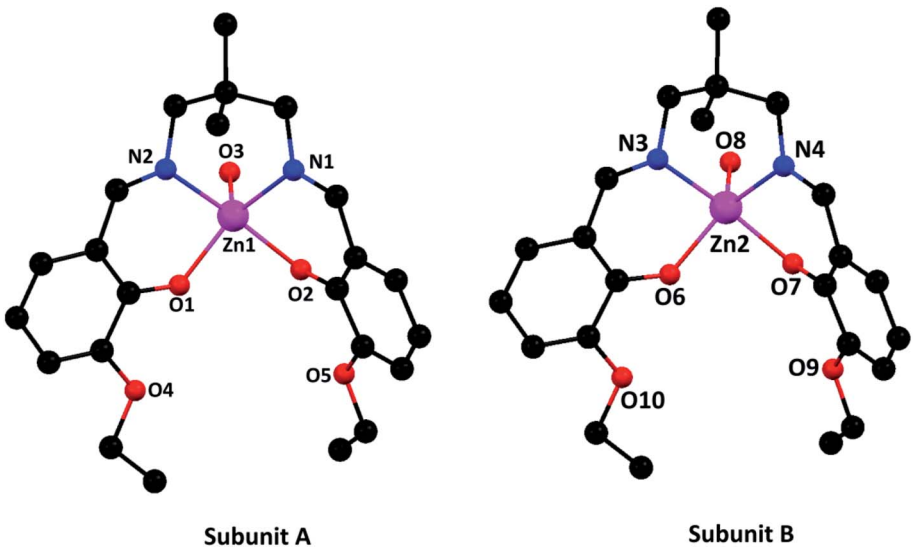

Fig. 1 Perspective views of the complex with selective atom numbering scheme. Hydrogen atoms and solvent molecules have been omitted for clarity.

Table 2 Selected bond lengths (Å) of the complex

Zn(1)–O(1)	2.037(4)	Zn(2)–O(6)	2.029(4)
Zn(1)–O(2)	1.998(4)	Zn(2)–O(7)	2.007(4)
Zn(1)–O(3)	2.005(4)	Zn(2)–O(8)	2.006(4)
Zn(1)–N(1)	2.107(4)	Zn(2)–N(3)	2.121(4)
Zn(1)–N(2)	2.113(5)	Zn(2)–N(4)	2.105(5)

Table 3 Selected bond angles (°) of the complex

O(1)–Zn(1)–O(2)	88.38(17)	O(6)–Zn(2)–O(7)	89.06(17)
O(1)–Zn(1)–O(3)	96.98(16)	O(6)–Zn(2)–O(8)	97.37(17)
O(1)–Zn(1)–N(1)	166.15(16)	O(6)–Zn(2)–N(3)	86.13(16)
O(1)–Zn(1)–N(2)	86.75(17)	O(6)–Zn(2)–N(4)	165.19(17)
O(2)–Zn(1)–O(3)	112.27(18)	O(7)–Zn(2)–O(8)	110.56(17)
O(2)–Zn(1)–N(1)	88.15(17)	O(7)–Zn(2)–N(3)	142.75(17)
O(2)–Zn(1)–N(2)	141.40(18)	O(7)–Zn(2)–N(4)	87.73(17)
O(3)–Zn(1)–N(1)	96.75(17)	O(8)–Zn(2)–N(3)	106.68(18)
O(3)–Zn(1)–N(2)	106.33(18)	O(8)–Zn(2)–N(4)	97.30(18)
N(1)–Zn(1)–N(2)	87.62(17)	N(3)–Zn(2)–N(4)	87.69(17)

assume chair conformations with puckering parameters,[61] q = 0.605(5) Å, θ = 6.3(5)°, φ = 138(4)° and q = 0.603(5) Å, θ = 6.8(5)°, φ = 277(4)°, respectively.

Hirshfeld surfaces analysis

The Hirshfeld surfaces of the complex is mapped over d_{norm} (range −0.1 Å to 1.5 Å), shape index and curvedness (Fig. 2). Red spots on the Hirshfeld surfaces mapped with d_{norm} denote the dominant interactions. Shape index can be used to identify complementary hollows (red) and bumps (blue) where two molecular surfaces touch one another. Curvedness is a function of the root-mean-square curvature of the surface and maps of curvedness typically show large regions of green (relatively flat) separated by dark blue edges (large positive curvature).

The intermolecular interactions appear as distinct spikes in the 2D fingerprint plot (Fig. 2). The main interactions are observed between the oxygen and hydrogen atoms (O···H). Other visible spots in Hirshfeld surfaces correspond to C···H contacts.

IR and electronic spectra

In the IR spectrum of the complex (Fig. 3), a distinct band appears around 1625 cm^{-1} due to stretching vibrations of azomethine (C=N) groups.[62] The bands in the range of 2840–2960 cm^{-1} due to alkyl C–H bond stretching vibrations are customarily noticed in the IR spectrum of the complex.[63] A distinct band is observed at 3351 cm^{-1} due to O–H stretching vibrations of coordinating water molecule and lattice water molecule.[64]

Electronic spectrum of the complex has been recorded in DMF medium. There are only three bands in the UV-vis spectrum of the complex. Bands at 232 nm and 272 nm may be attributed as $\pi \rightarrow \pi^*$ transitions.[65–67] The band at 356 nm may be attributed to the $n \rightarrow \pi^*$ charge transfer transition.[68,69] There is no band corresponding to d–d electronic transitions, as expected for zinc(II) complexes with d^{10} electronic configuration.[55]

^{1}H NMR spectrum

^{1}H NMR Spectra of complex is shown in Fig. 4. Imine protons (–CH=N) of the complex appeared as a singlet at 8.12 ppm. Aromatic protons of the complex have been noticed in the range of 6.24–6.74 ppm. The methylene protons of diamine moiety of the complex appeared as singlet at 3.46 ppm another methylene

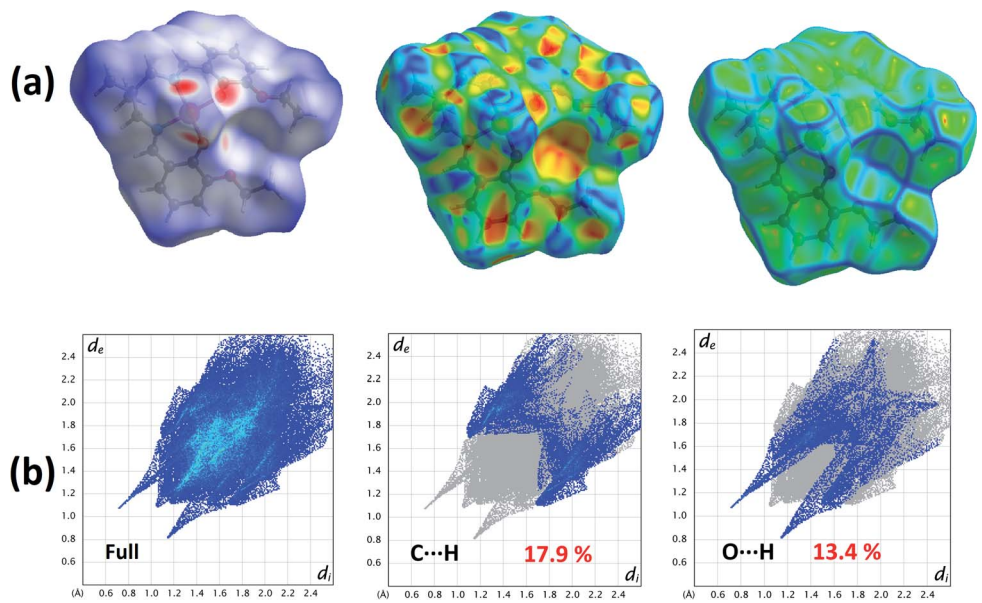

Fig. 2 (a) Hirshfeld surfaces of the complex mapped with d_{norm} (left), shape index (middle) and curvedness (right); (b) the proportion of O···H/H···O interactions comprise 13.4% of the Hirshfeld surfaces and the proportion of C···H/H···C interactions comprise 17.9% of the Hirshfeld surfaces.

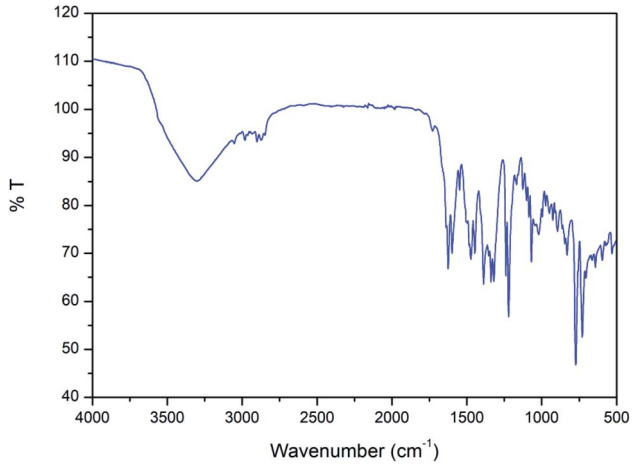

Fig. 3 IR spectrum of the complex.

protons of ethoxy group appeared as quartet in the range of 3.96–4.01 ppm. Methyl protons of ethoxy group appeared as triplet in the range of 1.21–1.24 ppm and another methyl protons of diamine appeared as singlet at 0.87 ppm.

DFT calculations. The theoretical study is focused to the analysis of the C–H$\cdots\pi$ interactions observed in the solid state of $[ZnL(H_2O)]\cdot H_2O$. Fig. 5 shows a partial view of the X-ray structure where an interesting 1D supramolecular assembly is highlighted. It propagates due to the formation of several C–H$\cdots\pi$ interactions involving the aliphatic linker 2,2-dimethyl-1,3-propanediyl moiety and both aromatic rings.

To rationalize the interaction, the MEP surface (Fig. 6) of $[ZnL(H_2O)]$ complex has first been computed since it is convenient to investigate the most nucleophilic and electrophilic groups of the complex. The MEP maximum is located at the H-atoms of the coordinated water molecule (+70 kcal mol^{-1}). This large MEP value is due to the enhanced acidity of water H-atoms upon complexation to Zn(II). The minimum is also very large (-74 kcal mol^{-1}) because it is located at the region where the four O-atoms of the ligand converge. Furthermore, the MEP values at the H-atoms of the methyl groups are positive (+12 and +18 kcal mol^{-1}) and those over the center of the phenoxido ligands are negative (-31 kcal mol^{-1}), thus anticipating a strong C–H$\cdots\pi$ interaction energies. Moreover, the van der Waals surface shows that the methyl group fits well into the cleft formed by both aromatic surfaces.

Fig. 7 shows a dimer extracted from the infinite 1D chain commented above (see Fig. 5) where the network of C–H$\cdots\pi$ interactions is represented. Four C–H$\cdots\pi$ contacts are formed with H$\cdots$C distances ranging from 3.30 to 3.56 Å, which are in the typical range described before for this type of bonding. One of the C–H bonds points to one exocyclic O-atom. The formation energy is very large $\Delta E = -13.9$ kcal mol^{-1} confirming the

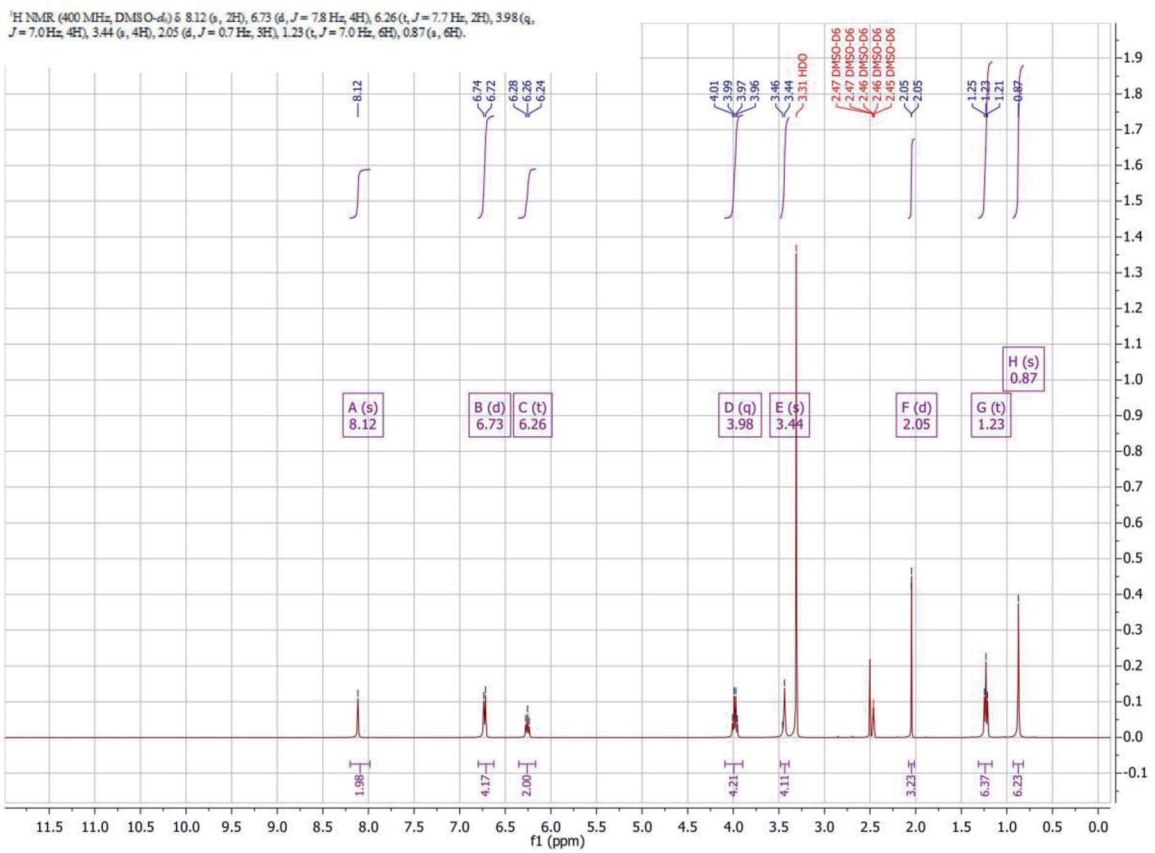

Fig. 4 ^{1}H NMR of the complex.

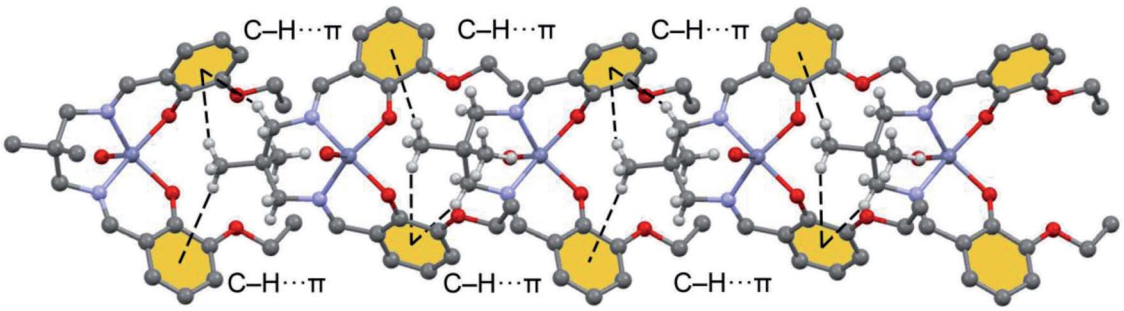

Fig. 5 Detail 1D infinite chain observed in the solid state of $[Zn(L)H_2O]\cdot H_2O$ with indication of the C–H···π interactions. H-atoms omitted for clarity apart from those of the aliphatic linker.

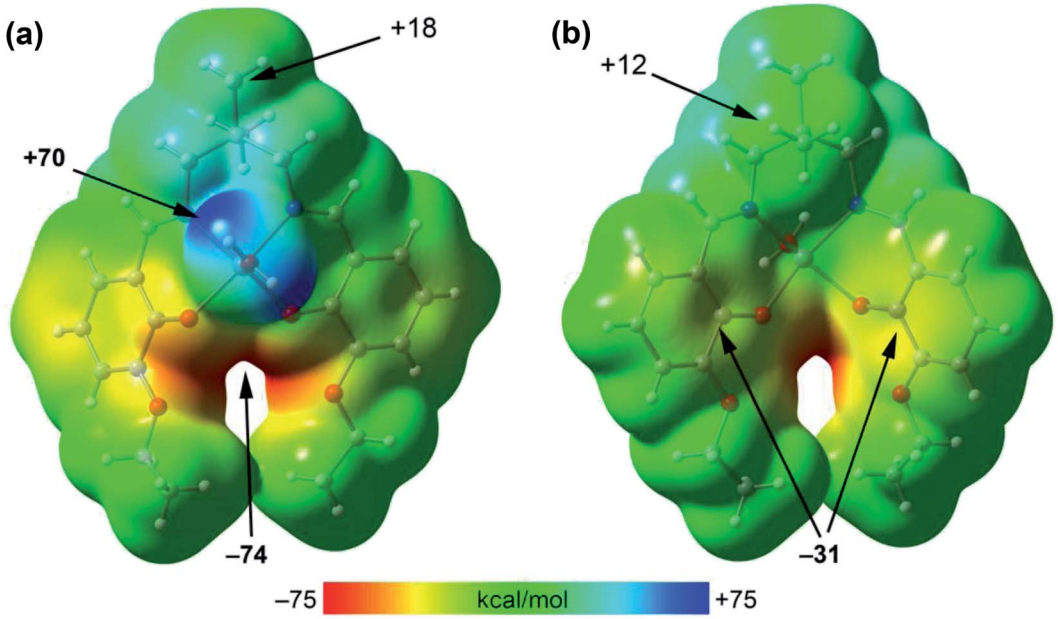

Fig. 6 MEP surface of f $[Zn(L)H_2O]$ complex at the PBE0-D3/def2-TZVP level of theory and using two different orientations: coordinated molecule pointing up (a) or down (b). The values at selected points of the surface are indicated in kcal mol^{-1}.

importance of this network of interactions in the solid state of $[ZnL(H_2O)]$.

The noncovalent interaction plot index (NCI Plot) has been used further to characterize the C–H···π assembly in $[ZnL(H_2O)]$. The NCI plot is an intuitive method that shows which spatial regions between molecules interact. Consequently, it is very convenient to analyze noncovalent interactions. Moreover, it gives hints regarding the strength of the interactions by using a colour code, where green is used for weak interactions and yellow for repulsive ones. Strongly attractive and repulsive interactions are represented by blue and red colors, respectively. The NCI plot of the dimer is given in Fig. 8, which confirms the existence of the C–H···π interactions that are characterized by several green isosurfaces located between the π-surfaces and the H-atoms. It also confirms the C–H···O contact also characterized by a green isosurface located between the C–H group and the O-atom of the ethoxy substituent. Despite all individual contacts are weak (green isosurface) the sum of all contributions is strong enough to dictate the formation of the 1D assembly shown in Fig. 5.

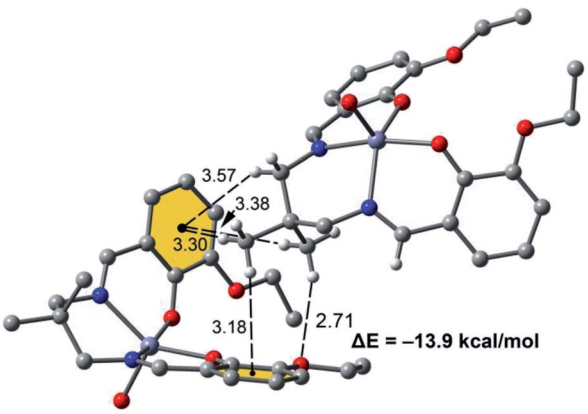

Fig. 7 Dimer of $[Zn(L)H_2O]$ with indication of the C–H···π interactions. Distances are in Å.

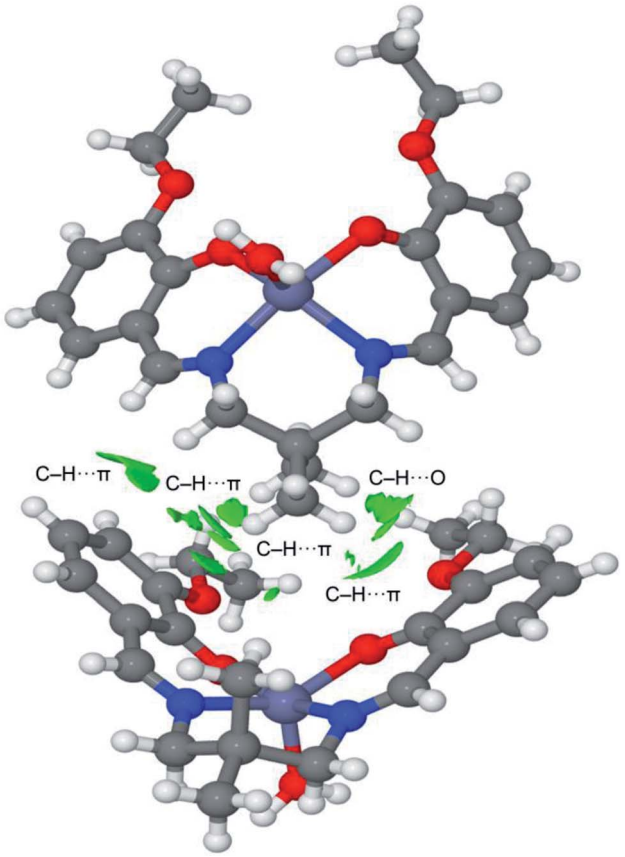

Fig. 8 NCI Plot of the dimer of [Zn(L)H_2O]. Isosurface 0.4 density cut-off 0.04 a.u. Colour scale -0.035 a.u. $\leq$ sign(λ_2) $\rho \leq 0.035$ a.u.

Concluding remarks

A zinc(II) complex, [ZnL(H_2O)]·H_2O {H_2L = 2,2′-[(2,2-dimethyl-1,3-propanediyl)bis(nitrilomethylidyne)]bis[6-ethoxyphenol]} has been synthesized and characterized by single crystal X-ray diffraction study, elemental analysis, FT-IR and electronic spectroscopic techniques. Crystal structure analysis reveals that C–H···π interactions lead to the formation of 1D supramolecular assembly in the solid state. The strength of the C–H···π interaction has been evaluated using DFT calculations and also analysed using the MEP surface and NCI plot index computational tool. The large dimerization energy confirms the importance of C–H···π interactions in the solid state of [ZnL(H_2O)]·H_2O.

Conflicts of interest

There are no conflicts to declare.

Acknowledgements

T. B. thanks the CSIR, India, for awarding a Senior Research Fellowship [Sanction No. 09/096(0861)/2016-EMR-I]. We also acknowledge the MCIU/AEI of Spain (project CTQ2017-85821-R, FEDER, UE funds) for financial support.

References

1 V. Stavila, A. A. Talin and M. D. Allendorf, *Chem. Soc. Rev.*, 2014, **43**, 5994–6010.
2 R.-G. Xiong, J.-L. Zuo, X.-Z. You, B. F. Abrahams, Z.-P. Bai, C.-M. Chec and H.-K. Fun, *Chem. Commun.*, 2000, 2061–2062.
3 M. D. Heinemann, R. Mainz, F. Österle, H. Rodriguez-Alvarez, D. Greiner, C. A. Kaufmann and T. Unold, *Sci. Rep.*, 2017, **7**, 45463.
4 V. Nishal, D. Singh, R. K. Saini, S. Bhagwan, V. Tanwar, Sonika, R. Srivastava and P. S. Kadya, *J. Mater. Sci.: Mater. Electron.*, 2015, **26**, 6762–6768.
5 H.-J. Son, W.-S. Han, J.-Y. Chun, B.-K. Kang, S.-N. Kwon, J. Ko, S. J. Han, C. Lee, S. J. Kim and S. O. Kang, *Inorg. Chem.*, 2008, **47**, 5666–5676.
6 R. T. Kuznetsova, I. V. Aksenova, A. A. Prokopenkoa, V. A. Pomogaev, E. V. Antina, M. B. Berezin, L. A. Antina and N. A. Bumagina, *J. Mol. Liq.*, 2019, **278**, 5–11.
7 T. Joshi, B. Graham and L. Spiccia, *Acc. Chem. Res.*, 2015, **48**, 2366–2379.
8 T. Basak, A. Bhattacharyya, M. Das, K. Harms, A. Bauzá, A. Frontera and S. Chattopadhyay, *ChemistrySelect*, 2017, **2**, 6286–6295.
9 M. Karmakar and S. Chattopadhyay, *Polyhedron*, 2020, **184**, 114527.
10 E. Y. Tirel, Z. Bellamy, H. Adams, V. Lebrun, F. Duarte and N. H. Williams, *Angew. Chem., Int. Ed.*, 2014, **53**, 8246–8250.
11 J. Huo, D. Yu, H. Li, B. Luoa and N. Arulsamy, *RSC Adv.*, 2019, **9**, 39323–39331.
12 T. Basak, M. G. B. Drew and S. Chattopadhyay, *Inorg. Chem. Commun.*, 2018, **98**, 92–98.
13 Y. Zhao, L. Wang, N.-N. Fan, M.-L. Han, G.-P. Yang and L.-F. Ma, *Cryst. Growth Des.*, 2018, **18**, 7114–7121.
14 S. Li Yao, S. Jun Liu, C. Cao, X.-M. Tian, M.-N. Bao and T.-F. Zheng, *J. Solid State Chem.*, 2019, **269**, 195–202.
15 M. Karmakar, S. Roy and S. Chattopadhyay, *New J. Chem.*, 2019, **43**, 10093–10102.
16 A. Das, S. Jana and A. Ghosh, *Cryst. Growth Des.*, 2018, **18**, 2335–2348.
17 S. Shanmugaraju, C. Dabadie, K. Byrne, A. J. Savyasachi, D. Umadevi, W. Schmitt, J. A. Kitchenc and T. Gunnlaugsson, *Chem. Sci.*, 2017, **8**, 1535–1546.
18 S. Roy, I. Mondal, K. Harms and S. Chattopadhyay, *Polyhedron*, 2019, **159**, 265–274.
19 M. Karmakar, T. Basak and S. Chattopadhyay, *New J. Chem.*, 2019, **43**, 4432–4443.
20 S. Dasgupta, E. Zangrando and I. Majumder, *ChemistrySelect*, 2017, **2**, 7073–7081.
21 A.-C. Chamayou, S. Ludeke, V. Brecht, T. B. Freedman, L. A. Nafie and C. Janiak, *Inorg. Chem.*, 2011, **50**, 11363–11374.
22 G. Parkin, *Chem. Rev.*, 2004, **104**, 699–767.
23 H. Sakiyama, R. Mochizuki, A. Sugawara, M. Sakamoto, Y. Nishida and M. Yamasaki, *J. Chem. Soc., Dalton Trans.*, 1999, 997–1000.
24 S. Aoki, M. Zulkefeli, M. Shiro and E. Kimura, *Proc. Natl. Acad. Sci. U. S. A.*, 2002, **9**, 4894–4899.

25 S. Roy, I. Mondal, K. Harms and S. Chattopadhyay, *Polyhedron*, 2019, **159**, 265–274.
26 T. Basak, R. M. Gomila, A. Frontera and S. Chattopadhyay, *CrystEngComm*, 2021, **23**, 2703–2710.
27 M. Kondo, T. Yoshitomi, K. Seki, H. Matsuzaka and S. Kitagawa, *Angew. Chem., Int. Ed.*, 1997, **36**, 1725–1727.
28 M. Schmittel and S. Saha, *Adv. Inorg. Chem.*, 2018, **71**, 135–175.
29 M. Karmakar, A. Frontera and S. Chattopadhyay, *CrystEngComm*, 2021, **23**, 1918–1928.
30 M. Nisa, M. Sirajuddin, S. Ali, M. N. Tahir and M. Iqbal, *Polyhedron*, 2020, **177**, 114273.
31 T. Basak, A. Bhattacharyya, K. Harms and S. Chattopadhyay, *Polyhedron*, 2019, **157**, 449–457.
32 G. R. Desiraju, *Angew. Chem., Int. Ed.*, 2007, **46**, 8342–8356.
33 C. B. Aakeröy and K. R. Seddon, *Chem. Soc. Rev.*, 1993, **22**, 397–407.
34 S. Saha, M. K. Mishra, C. M. Reddy, C. Malla and G. R. Desiraju, *Acc. Chem. Res.*, 2008, **51**, 2957–2967.
35 M. Nishio, M. Hirota and Y. Umezawa, *The CH/π Interaction*, Wiley-VCH, New York, 1998.
36 M. Nishio, *Phys. Chem. Chem. Phys.*, 2011, **13**, 13873–13900.
37 C. R. Bhattacharjee, G. Das, P. Mondal and N. V. S. Rao, *Polyhedron*, 2010, **29**, 3089–3096.
38 J. Gradinaru, A. Forni, V. Druta, F. Tessore, S. Zecchin, S. Quici and N. Garbalau, *Inorg. Chem.*, 2007, **46**, 884–895.
39 I. Mondal, T. Basak, S. Banerjee and S. Chattopadhyay, *CrystEngComm*, 2020, **22**, 3005–3019.
40 X.-X. Zhou, H.-C. Fang, Y.-Y. Ge, Z. Yuan Zhou, Z.-G. Gu, X. Gong, G. Zhao, Q.-G. Zhan, R.-H. Zeng and Y.-P. Cai, *Cryst. Growth Des.*, 2010, **10**, 4014–4022.
41 G. M. Sheldrick, *Acta Crystallogr., Sect. C: Cryst. Struct. Commun.*, 2015, **71**, 3–8.
42 G. M. Sheldrick, *SADABS, V2014/5, Software for Empirical Absorption Correction*, University of Göttingen, Institute fur Anorganische Chemieder Universitat, Gottingen, Germany, 1999–2003.
43 M. A. Spackman and D. Jayatilaka, *CrystEngComm*, 2009, **11**, 19.
44 F. L. Hirshfeld, *Theor. Chim. Acta*, 1977, **44**, 129.
45 H. F. Clausen, M. S. Chevallier, M. A. Spackman and B. B. Iversen, *New J. Chem.*, 2010, **34**, 193.
46 A. L. Rohl, M. Moret, W. Kaminsky, K. Claborn, J. J. McKinnon and B. Kahr, *Cryst. Growth Des.*, 2008, **8**, 4517.
47 A. Parkin, G. Barr, W. Dong, C. J. Gilmore, D. Jayatilaka, J. J. McKinnon, M. A. Spackman and C. C. Wilson, *CrystEngComm*, 2007, **9**, 648.
48 M. A. Spackman and J. J. McKinnon, *CrystEngComm*, 2002, **4**, 378.
49 S. K. Wolff, D. J. Grimwood, J. J. McKinnon, D. Jayatilaka and M. A. Spackman, *Crystal Explorer 2.0*, University of Western Australia, Perth, Australia, 2007, http://hirshfeldsurfacenet.blogspot.com.
50 F. H. Allen, O. Kennard, D. G. Watson, L. Brammer, A. G. Orpen and R. J. Taylor, *J. Chem. Soc., Perkin Trans. 1*, 1987, **2**, S1.
51 J. J. Kinnon, M. A. Spackman and A. S. Mitchell, *Acta Crystallogr., Sect. B: Struct. Sci.*, 2004, **60**, 627.
52 C. Adamo and V. Barone, *J. Chem. Phys.*, 1999, **110**, 6158–6170.
53 F. Weigend, *Phys. Chem. Chem. Phys.*, 2006, **8**, 1057.
54 S. Grimme, J. Antony, S. Ehrlich and H. Krieg, *J. Chem. Phys.*, 2010, **132**, 154104.
55 M. J. Frisch, G. W. Trucks, H. B. Schlegel, G. E. Scuseria, M. A. Robb, J. R. Cheeseman, G. Scalmani, V. Barone, G. A. Petersson, H. Nakatsuji, X. Li, M. Caricato, A. V. Marenich, J. Bloino, B. G. Janesko, R. Gomperts, B. Mennucci, H. P. Hratchian, J. V. Ortiz, A. F. Izmaylov, J. L. Sonnenberg, D. Williams-Young, F. Ding, F. Lipparini, F. Egidi, J. Goings, B. Peng, A. Petrone, T. Henderson, D. Ranasinghe, V. G. Zakrzewski, J. Gao, N. Rega, G. Zheng, W. Liang, M. Hada, M. Ehara, K. Toyota, R. Fukuda, J. Hasegawa, M. Ishida, T. Nakajima, Y. Honda, O. Kitao, H. Nakai, T. Vreven, K. Throssell, J. A. Montgomery Jr, J. E. Peralta, F. Ogliaro, M. J. Bearpark, J. J. Heyd, E. N. Brothers, K. N. Kudin, V. N. Staroverov, T. A. Keith, R. Kobayashi, J. Normand, K. Raghavachari, A. P. Rendell, J. C. Burant, S. S. Iyengar, J. Tomasi, M. Cossi, J. M. Millam, M. Klene, C. Adamo, R. Cammi, J. W. Ochterski, R. L. Martin, K. Morokuma, O. Farkas, J. B. Foresman and D. J. Fox, *Gaussian 16, Revision C.01*, Gaussian, Inc., Wallingford CT, 2016.
56 S. F. Boys and F. Bernardi, *Mol. Phys.*, 1970, **19**, 553.
57 J. Contreras-Garcia, E. R. Johnson, S. Keinan, R. Chaudret, J. P. Piquemal, D. N. Beratan and W. Yang, *J. Chem. Theory Comput.*, 2011, **7**, 625.
58 T. Basak, K. Ghosh and S. Chattopadhyay, *Polyhedron*, 2018, **146**, 81–92.
59 A. W. Addison, T. N. Rao, J. Reedijk, J. van Rijn and G. C. Verschoor, *J Chem. Soc., Dalton Trans*, 1984, 1349–1356.
60 S. Roy, S. Bhattacharya and S. Chattopadhyay, *J. Coord. Chem.*, 2016, **69**, 112–122.
61 D. Cremer and J. A. Pople, *J. Am. Chem. Soc.*, 1975, **97**, 1354–1358.
62 T. Basak, D. Das, P. P. Ray, S. Banerjee and S. Chattopadhyay, *CrystEngComm*, 2020, **22**, 5170–5181.
63 S. Roy, T. Basak, S. Khan, M. G. B. Drew, A. Bauzá, A. Frontera and S. Chattopadhyay, *ChemistrySelect*, 2017, **2**, 9336–9343.
64 T. K. Ghosh, S. Jana and A. Ghosh, *Inorg. Chem.*, 2018, **57**, 15216–15228.
65 T. Basak, C. J. Gòmez-Garcia, R. M. Gomila, A. Frontera and S. Chattopadhyay, *RSC Adv.*, 2021, **11**, 3315–3323.
66 S. Roy, M. G. B. Drew, A. Bauzá, A. Frontera and S. Chattopadhyay, *New J. Chem.*, 2018, **42**, 6062–6076.
67 D. N. Kumar and B. S. Garg, *Spectrochim. Acta, Part A*, 2006, **64**, 141–147.
68 T. Basak, A. Frontera and S. Chattopadhy, *Inorg. Chim. Acta*, 2021, **516**, 120081.
69 V. Nishal, D. Singh, A. Kumar, V. Tanwar, I. Singh, R. Srivastava and P. Singh Kadyan, *J. Org. Semicond.*, 2014, **2**, 15–20.